A point cloud based method for radiation source representation for cutting operation in the decommissioning of nuclear facilities

CHAO Nan[1], LIU Yong-kuo[2], XIA Hong[3], and YANG Li-qun[4]

1. Harbin Engineering University, Nantong street NO. 145, Harbin, 150001, China (chaonan@hrbeu.edu.cn)
2. Harbin Engineering University, Nantong street NO. 145, Harbin, 150001, China (LYK08@126.com)
3. Harbin Engineering University, Nantong street NO. 145, Harbin, 150001, China (xiahong@hrbeu.edu.cn)
4. Harbin Engineering University, Nantong street NO. 145, Harbin, 150001, China (hanyangrensheng@163.com)

Abstract: Nuclear decommissioning tasks involve a large number of cutting activities and result in a frequent change in the structure and produce many irregular objects. It is necessary to assess the dose rate for cutting operation before work to ensure the radiation safety of the staff. The paper presents a flexible radiation source representation method of gamma dose assessment method for cutting operation based on virtual reality technology and Point-Kernel method, and it can be applied to arbitrary geometries. The initial geometry of the radiation source is designed with the three-dimensional computer-aided design tools, and a point cloud model is generated automatically to represent the radiation source. When the cutting operation is performed, the point cloud models of cutting products are generated automatically by dividing the origin point cloud model according to the cutting surface. Then the generated point cloud model is simplified adaptively according to the position of the detecting point, and dose rates can be calculated with the Point-Kernel method. The flexibility and effectiveness of the proposed method was verified by simulating the cutting of different geometries, and the time and dose rate results were compared with that derived from VRBM and MCNP code.
Keyword: dose assessment; point cloud model; point kernel method; cutting operation; nuclear facilities decommissioning

1 Introduction

During the decommissioning of nuclear facilities, occupation workers face the risk of excessive radiation exposure, so it is necessary to perform dose assessment and safety analysis before personnel work. However, a large number of cutting and demolition activities required to be performed during the decommissioning process, which results in a frequent change in the structure and produce many irregular objects, making it difficult to perform safety analysis in such environments. Therefore, it is necessary to provide a flexible method of radiation source representation for cutting operation in the decommissioning of nuclear facilities to improve the efficiency and reliability of work analysis.

The Monte Carlo and the Point-Kernel method are commonly used for calculating radiation shield effectiveness and dose rates. The time efficiency is important in the dose assessment work during the cutting operation. Since the Monte Carlo method suffers from long computing time, it has limitations in dealing with the high time requirement issue. To tackle the time issue, the Point-Kernel method is usually used for dose assessment. Some researchers have studied the application of virtual reality (VR) in nuclear facilities decommissioning such as the ALARA (as low as reasonably achievable) planning tool VISIPLAN [1], and the three-dimensional simulation tool VR dose Planner system [2]. These programs were developed based on VR technology and Point-Kernel method. However, the scenarios need to be simplified with basic geometries.

In order to modeling the complex geometry efficiently, Vela took the advantage of the modeling capabilities of computer-aided design (CAD) tools to construct the geometry, and a code CIDEC was developed [3]. It can only deal with volumetric sources, and the accuracy of the method is ensured up to the grid resolution. Since the number of grid points grows cubically with the resolution, so does the computational effort.

Received date: November 3, 2018
(Revised date: January 10, 2019)

To cope with both accuracy and time requirements, Caracena presented an algorithm to calculate gamma dose rates for VR simulation applications in nuclear safeguards and security by calculating dose rates via a non-regular mesh model [4]. Moreover, to improve the efficiency, Caracena developed a KD-tree based method for fast radiation source representation [5]. However, geometries are restricted to parallelepipeds. Chao proposed a VR-based method (VRBM) to assess dose rates on arbitrary geometries [6]. To take both accuracy and time efficiency into account for irregular geometries, Chao developed a dose assessment method for cutting operation based on VRBM [7]. However, the number of point kernels need to be further simplified.

In addition, some researchers have developed some system for cutting simulation during the decommissioning of nuclear facilities. Park studied a dismantling digital mock-up system to simulate the decommissioning of nuclear facilities [8], while the cutting scenario is pre-designed and unchangeable. In order to overcome this restriction, Kim and Hyun simulated the cutting process based on a commercial system and digital manufacturing platform respectively [9][10]. Furthermore, Zhang developed a simulation system based on DELMIA and VIRTOOLS [11]. However, these methods didn't take the dose assessment into account.

In order to cope with both accuracy and time efficiency for dose calculation with complex geometries, this paper proposed a flexible and efficient radiation source representation method for dose assessment for the cutting operation based on virtual reality technology and Point-Kernel method. The method employs the point cloud model to represent radiation sources, and allows for the automatic modeling and simplification of radiation sources with arbitrary geometries. The point cloud based method (PCBM) uses computer-aided design (CAD) tools, such as 3ds Max, to design the initial geometric model. When the initial geometric model is loaded, the point cloud model of the radiation source is generated automatically. When the cutting operation is performed, the point cloud models of cutting products are generated automatically by dividing the origin point cloud model according to the cutting surface, and then the adaptive point kernels are generated by simplifying the point cloud model according to the detecting position to improve the time efficiency while keeping accuracy. Ultimately, the dose rates are calculated with the Point-Kernel method. The method makes it possible to assess dose rates for arbitrary geometries and radiation sources for cutting operation efficiently during the nuclear facilities decommissioning.

2 Point kernel method

The Main idea of Point-Kernel method is that the radiation source can be seen as consisting of a series of discrete point kernels, and the dose rate at the detecting point is composed of the contributions of all point kernels to the detecting point [12]. The total dose rate from a point kernel isotropic with energy E to the detecting point is given by:

$$D(r,E) = C(E)S(E)B\big(E,t(E)\big)\frac{e^{-t(E)}}{4\pi r^2} \quad (1)$$

Where r is the distance from the point kernel to the detecting point, C is gamma flux density to dose rate conversion factor, S is the strength of the point kernel, B is the buildup factor, which can be obtained from the Geometric-Progression formula. The mean free paths, t, between the point kernel and the detecting point can be calculated with the following equation

$$t(E) = \sum_{i=1}^{n} \mu_i(E) d_i \quad (2)$$

Where i is the index of the space region, n is the number of regions, μ_i is the linear attenuation factor for i-th region, and d_i is the section of the line between the detecting point and the point kernel in the i-th region.

Therefore, the total dose rate at the detecting point can be calculated by integration of equation (1) over the source volume V and integration over the energies E of radiation spectrum

$$D = \int_0^{E_{max}} dE \iiint_V^v D(r,E)dr \quad (3)$$

3 Methodology

3.1 The generation of point cloud model

Prior to dose calculation, we need to obtain the geometry of the object. The initial geometric models are designed in the CAD tools. The surface of the object is composed of triangular faces, and all these faces constitute the mesh model of the object. For each triangular face, the positive direction of its

normal is always pointing to the outside of the object. When the object is loaded, the material and radiometric attributes are inputted, and then the point cloud model is generated automatically by sampling the space.

The schematic diagram of the point cloud model generation for volumetric radiation sources is shown in Fig.1. The bounding box of the object is selected as the sampling space, so the total number N of samples should be $N=De\times V$, where V is the volume of the sampling space, and De is the sampling density. Of course, the other kinds of sampling space that contain the object can also be chosen, and the smaller the space, the higher the sampling efficiency.

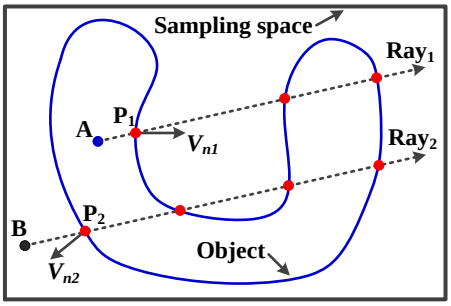

Fig.1 Two-dimensional graph showing the point cloud model generation for volumetric radiation sources. The point A and B are samples. The dash lines with arrow are the rays starting from the point A and B respectively. The intersections between the rays and the object are shown in red points. The point P1 is the nearest intersection of A, and P2 is the nearest intersection of B. The normal of the object at P1 and P2 are Vn1 and Vn2 respectively. A is inside the object, and $\overrightarrow{AP_1}\cdot V_{n1}>0$. B is outside the object, and $\overrightarrow{BP_2}\cdot V_{n2}<0$.

The procedure for the point cloud model generation for volumetric radiation sources is shown in Fig.2. The point set Q is used to store the point cloud data First, a point P is obtained by sampling the space, and then a ray in arbitrary direction is created by setting P as the starting point, and the intersections between the object and the ray constitute a point set J. If J is empty, it means that the ray doesn't collide with the object, so P is outside the object and abandoned; otherwise, the nearest point P_1 of P is selected from J, and the normal of the triangular face on which P_1 is located is denoted as V_n. If the inner product between the vector $\overrightarrow{PP_1}$ and V_n is larger than zero, that is $\overrightarrow{PP_1}\cdot V_n>0$, it means that the angle between $\overrightarrow{PP_1}$ and V_n is less than 90 degrees, and P is inside the object, so P is taken as a valid sample and put into the point set Q. The process above keeps repeating until the sampling times reach to the threshold N. Ultimately, all the points in Q form the point cloud model of the object.

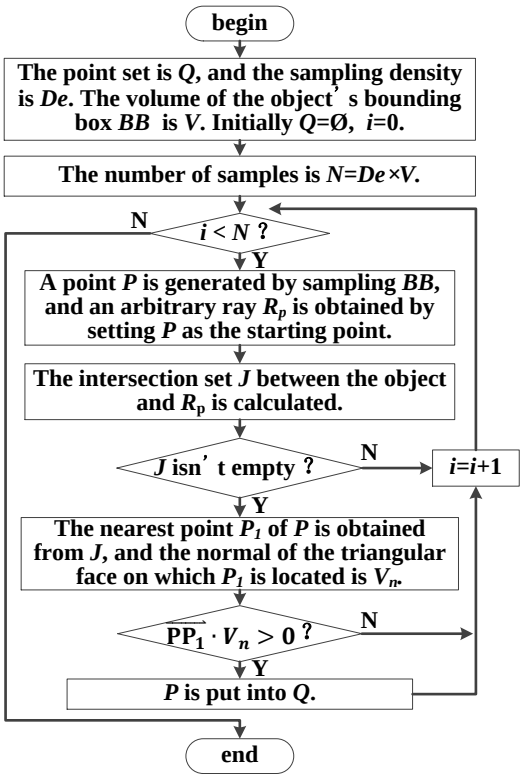

Fig.2 The procedure of the point cloud model generation for volumetric radiation sources.

Similarly, since the object's mesh is composed of triangular faces, when the object is a surface radiation source, the point cloud model can be obtained by sampling these triangular faces.

3.2 Cutting operation on point cloud model

When the cutting operation is performed, the point cloud model of the object is divided into two sub-point cloud models by the cutting surface, and the two parts are the discrete representation of the cut products. The method of point cloud division is shown in Fig.3.

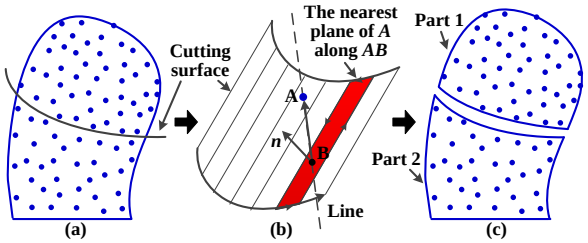

Fig.3 Schematic diagram of the point cloud division.

The cutting surface can be approximated as a set of rectangular faces as shown in Fig.3 (b), so cutting operation can be accomplished by determining which side of the cutting surface the points of the point cloud model belongs to. We opined that the positive normal of each rectangular face satisfies the right-hand rule along the cutting trajectory around the rectangle. First, a point A is selected from the point cloud model, and then a line is created by passing through A and a point B on the cutting surface. The nearest intersection F of A and the corresponding rectangular face with the normal $\boldsymbol{n}$ are selected to judge the relationship between the point A and the cutting surface as shown in Fig.3 (b). If the dot product of vector $\overrightarrow{BA}$ with n is larger than zero, that is, $\overrightarrow{BA} \cdot n>0$, then the point A is on the upper side of the cutting surface; otherwise, it is on the lower side. Then another point in the point cloud model is selected to perform the above steps until all the points are processed. Ultimately, the original point cloud model of the object is divided into two parts, and each part becomes the new point cloud model of the cutting products.

3.3 The generation of adaptive point kernels and dose calculation

Since the object is represented with the point cloud data, the general approach is to treat each point as a point kernel for dose assessment, which is applied in VRBM. It can ensure the accuracy of the result, but requires a long calculation time. In order to maintain the accuracy while improving the computational efficiency, the point cloud model need to be simplified adaptively to reduce the number of point kernels used for dose assessment. The basic idea of the simplification is to divide the point cloud into a series of sub-point clouds, and then a point kernel is generated at the center of each sub-point cloud to represent the attributes of this sub-point cloud. The method of adaptive point kernel generation is shown in Fig.4.

A scale factor, a, belongs to the interval 0 to 1 is defined, that $a\in(0,1)$. For a point E in space, the distance between the detecting point and E is denoted as d. A voxel V_E that contains E with any shape is applied, and the maximum size of V_E is denoted as d_E. It is defined that when d_E is less than or equal to the product of a with d, that $d_E \leq a \times d$, the voxel V_E can be seen as a point. The larger of a, the less of the number of point kernels to represent the radiation source, so does the calculating time, while the larger error is introduced. The scale factor a can be adjusted based on the importance of accuracy and time. The paper uses the cuboid to split the point cloud model, so the d_E is equal to the maximum diagonal length of the cuboid, and the d is the distance between the center of the cuboid and the detecting point.

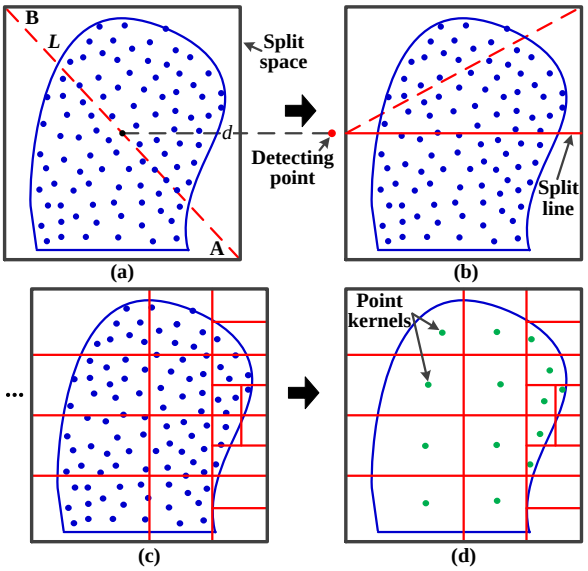

Fig.4 Two-dimensional graph showing the method of adaptive point kernel generation. The dash line AB is the maximum diagonal length of the cuboid, and the blue points are the point cloud data, and the split line is shown in solid red line, and the point kernel is shown in green. The initial split space is shown in (a), and its center is shown in black point. The initial split space is divided into two parts by a split line in (b). All the existing cuboids needn't be divided in (c), and each point kernel is generated at the center of the points inside each cuboid in (d).

The procedure for the adaptive point kernel generation is shown in Fig.5. First, the object's bounding-box is selected as the initial split space, and

the split threshold is denoted as *TH*, and point kernel set is *KS*. In each iteration, the original cuboid space is divided into two cuboids with the same size by a split plane located at the center of the longest axis and perpendicular to the longest axis, and then the maximum diagonal length L of each cuboid is checked whether it larger than the split threshold *TH* and the product of the factor a with the distance d. If $L \le a \times d$ or $L \le TH$, it means that the cuboid can be seen as a point or it reach to the split threshold, and then all the points inside the cuboid form a sub-point cloud, and a point kernel K is generated at the center of these points and put into *KS*; otherwise, it means that the cuboid needs a further division, so it is stored in the set of cuboids to be divided. Once a cuboid is divided, it is destroyed and no longer exists anymore. The above process keeps repeating until all the existing cuboids needn't be divided. Ultimately, all the points in *KS* constitute the adaptively distributed point kernels, which can deal with arbitrary geometries.

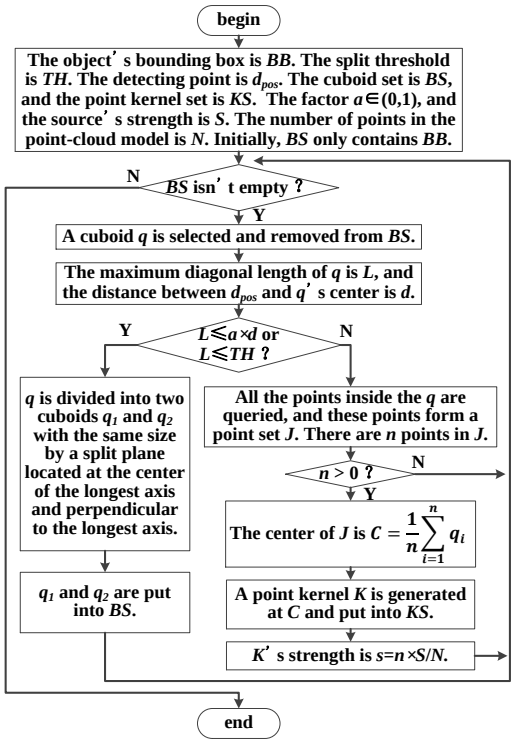

Fig.5 The procedure for the adaptive point kernel generation.

After the point cloud models of the cutting products are obtained. The number of points in the original point cloud model is denoted as N. The averaged strength of the i-th point kernel s_i can be calculated using equation (4)

$$s_i = K_i \cdot S/N \tag{4}$$

Where S is the strength of the original source, K_i is the number of points in the sub-point cloud that constitute the i-th point kernel.

Then equation (3) can be approximately as follows

$$D(r_d) \approx \sum_{i=1}^{n} s_i \sum_{j=1}^{m} C(E_j)P(E_j)B\left(E_j, t_i(E_j)\right)\frac{e^{-t_i(E_j)}}{4\pi r_i^2} \tag{5}$$

where r_d is the detecting point, n is the number of point kernels, s_i is the strength of the i-th point kernel, m is the number of energy E of radiation spectrum, $P(E_j)$ is the probability that the source emits photons with energy E_j, C is gamma flux density to dose rate conversion factor, B is the buildup factor, t is the mean free paths between the point kernel and the detecting point, r is the distance from the point kernel to the detecting point.

Taking into account the computational efficiency of the point acquisition, the octree [13] is used to query the points inside a cuboid, which can query points quickly and accurately in the three-dimensional space.

4 Simulations and results

This section is devoted to an experimental study of the dose assessment method considered in the paper. All methods were run on a computer with 3.3 GHz processor and 8 GB RAM on Windows operating system. The scalar factor a, is taken as 1/5 in the calculations, and the results were compared with that derived from VRBM and MCNP code.

4.1 Basic geometries modeling test

The first set of simulations was run to illustrate the geometric modeling capability of the method. Eight kinds of basic geometries were used, and they are cone, sphere, hemisphere, cylinder, parallelepiped, tube, U-shaped tube and cylindrical surface, where the convex surface, a concave surface, flat surface and their combination were considered. Some of these geometries have been used as benchmark cases in VRBM, and more complex geometries can be composed of these basic geometries.

Figure 6 presents the point cloud model generation and cutting snapshots. To generate an irregular

geometry, a curved cutting surface is used to divide the object. It can be observed that the point cloud models can give good representations of these objects, and the cutting operation generated the point cloud models of the cutting products successfully, and the combinations of the cut products are also consistent with the original models.

Figure 7 shows the adaptive point kernel generation snapshots. The test objects are the same as those shown in Fig.6, and the detecting points are located at right of these geometries and 15 cm away from their center. We can see that the number of generated point kernels is adaptive to the distance between the detecting point and the source, and the point kernels near the detecting point are densely distributed, and the farther away from the detecting point, the more sparsely distributed, so the PCBM has the ability to generate adaptive point kernels and deal with arbitrary geometries.

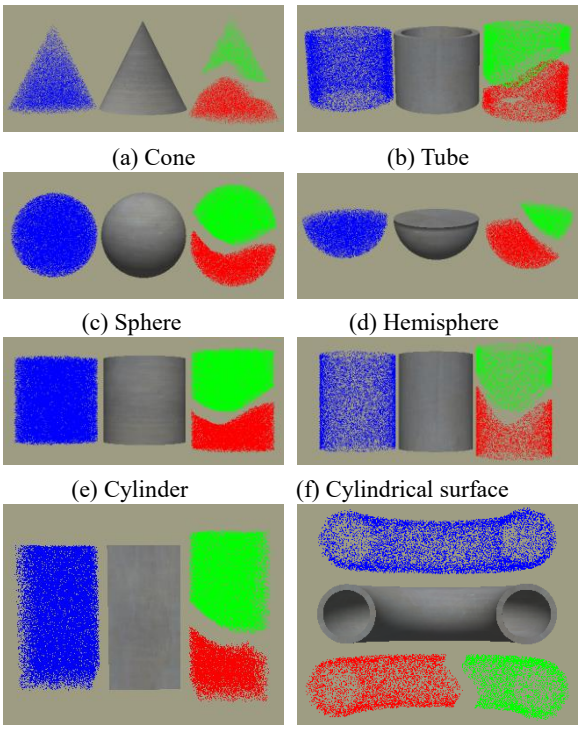

Fig.6 Point cloud model generation and cutting snapshots. The object is in the middle, and the left model (the upper in (h)) is the point cloud model, and the right model (the below in (h)) is the point cloud models of the cutting products.

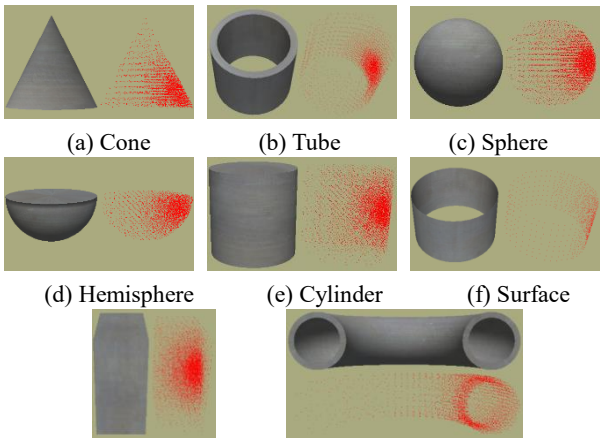

Fig.7 Adaptive point kernel generation snapshots.

4.2 Time efficiency of dose rate calculation test

The second sets of simulations were aim at demonstrating the time efficiency of dose rate calculation of PCBM, especially in comparison with the VRBM's models.

The basic case is that a 100×100×100 cuboid is positioned at the origin of coordinates aligned with the axis in a room filled with air. The source is composed of Cs^{137} and Co^{60}, and the 2 cm water shielding was placed in the x-axes and 2 cm away from the source surface.

The number ratio of point kernel and running time ratio of PCBM to VRBM versus the distance between the detecting point and the cuboid's center is shown in Fig.8. It can be observed that the number and running time ratio of PCBM to VRBM decreases with the increase in the distance between the detecting point and the source. This phenomenon is because VRBM applies dense uniform point kernels for calculation, and uses the same set of point kernels to calculate dose rates of different detecting points, and this technique is useful to maintain a good accuracy but inefficiency. By contrast, PCBM uses adaptive strategy to generate point kernels, and the farther away from the source, the more obvious advantage of PCBM's running time, and the time radio of PCBM to VRBM can even reach 2.5%, proving a better time performance of PCBM.

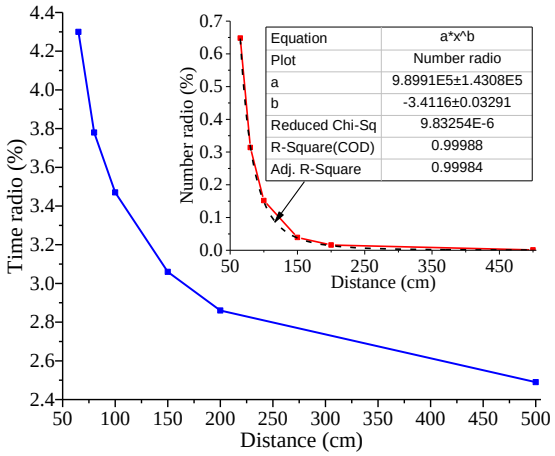

Fig.8 The number and running time ratio of PCBM to VRBM versus the distance between the detecting point and the center of the cuboid. The results were averaged over 100 runs with the discrete density of 1cm^{-3}.

4.3 Accuracy of dose rate calculation test

The third sets of simulations were designed to illustrate the accuracy performance of PCBM compared with VRBM and MCNP. Four basis shieling cases were considered in the test, which were already used as benchmark cases in dose rate calculations in CIDEC and VRBM. The results of MCNP were generated by running the code for two hours, and that of PCBM and VRBM were averaged over 100 times.

The basis case is that a 20×20×20 cm cubic source is positioned at the origin of coordinates aligned with the axis, and it was located in a room filled with air. The source is a ^{137}Cs with the activity of 4.353×10^{10} Bq, and only the 0.662 MeV emission line of the isotope was considered. The source is distributed in the air. Both the thin layer (0.2 cm) and thick layer (2.0 cm) were considered in the materials of water and lead. The shielding was placed in the x-axes, 5 cm away from the source surface.

Table 1 presents the results of PCBM, VRBM and MCNP. It can be seen that the maximum relative deviation of PCBM to the result of VRBM is 0.1% and all the deviations are less than 1.0%. In addition, the maximum relative deviation to MCNP is 11.35%, and most of the deviations are less than 10.0%. The results show acceptable correlation with the results of VRBM and MCNP.

Table 1 Results from PCBM, VRBM and MCNP in shielding case.

				Compared with VRBM		Compared with MCNP	
Shield	Material	Calculated positions	PCBM (mSv/h)	VRBM (mSv/h)	Deviation from VRBM (%)	MCNP (mSv/h)	Deviation from MCNP (%)
Thin layer (0.2cm thick)	Water	(20,0,0)	85.95	85.99	0.05	95.55	10.05
		(50,0,0)	13.26	13.26	0.00	14.68	9.67
		(100,0,0)	3.28	3.28	0.00	3.70	11.35
	Lead	(20,0,0)	71.97	71.99	0.03	80.12	10.17
		(50,0,0)	11.32	11.33	0.09	12.59	10.09
		(100,0,0)	2.81	2.81	0.00	3.16	11.08
Thick layer (2cm thick)	Water	(20,0,0)	84.73	84.76	0.04	89.52	5.35
		(50,0,0)	13.08	13.09	0.08	13.90	5.90
		(100,0,0)	3.24	3.24	0.00	3.54	8.47
	Lead	(20,0,0)	10.00	9.99	0.10	11.12	10.07
		(50,0,0)	1.92	1.92	0.00	2.09	8.13
		(100,0,0)	4.88×10^{-1}	4.88×10^{-1}	0.00	0.53	7.92

5 Discussion

In this paper, we try to use the virtual reality technology to improve the geometric modeling capacity and efficiency of the dose assessment in the process of cutting tasks during the decommissioning of nuclear facilities, and presented a point cloud-based radiation source representation method for cutting operation. The proposed method can automatically generate the point cloud model of the radiation source without considering its specific shape, and can deal with arbitrary geometries, so the modeling process is more flexible and efficient. Moreover, it has the ability to generate adaptive point kernels for arbitrary geometry by adaptively simplifying the point cloud model according to the detecting position, which can improve the time efficiency while keeping accuracy.

However, it was observed that the method presented in this paper only realizes the point cloud generation of the cutting product, and does not consider the reconstruction of the surfaces of the cutting products. Consequently, our next research work will focus on developing an efficient reconstructing solution of the surfaces of the cutting products to improve the simulation capabilities of the method.

6 Conclusion

A flexible point-cloud-based radiation source representation method has been developed for dose assessment in the cutting operation during the decommissioning of nuclear facilities. The method is based on the virtual reality and Point-Kernel method and called PCBM, and it has been tested by simulating the cutting of different geometries and comparing it with VRBM and MCNP code.

The geometric modeling capability of PCBM was verified by simulating the cutting operation of basic geometries, and the results show that the PCBM has a good performance in modeling complex geometries. The time efficiency of PCBM was compared with that of VRBM, and the results illustrate that PCBM can generates adaptive point kernels automatically according to the detecting position, and the running time ratio of PCBM to VRBM decrease as the distance increases, and it can even reach 2.5%, showing a good time performance of PCBM. Dose calculation results of PCBM are compared with those from VRBM and MCNP code, and the results show good correlations between PCBM and the results from VRBM and MCNP, demonstrating the accuracy of the method. The work makes it possible to perform a flexible and efficient dose assessment in a dynamic environment during the decommissioning of nuclear facilities.

Acknowledgement

This research work was funded by the Natural Science Foundation of Heilongjiang Province, China (Grant Nos. A2016002), the Foundation of Science and Technology on Reactor System Design Technology Laboratory (HT-KFKT-14-2017003), and the project of Research Institute of Nuclear Power Operation (No. RIN180149-SCCG).

References

[1] VERMEERSCH, F., and BOSSTRAETEN, C.V.: Development of the VISIPLAN ALARA planning tool. Proceeding of the International Conference on Topical Issues in Nuclear Radiation and Radioactive Waste Safety, 1998:4-31.

[2] SZŐKE, I., LOUKA, M.N., BRYNTESEN, T.R., EDVARDSEN, S.T., and BRATTELI, J.: Comprehensive support for nuclear decommissioning based on 3D simulation and advanced user interface technologies, J. Nucl. Sci. Technol., 2015, 52:371-387.

[3] VELA, O., BURGOS, E.D., and PEREZ, J.M.: Dose rate assessment in complex geometries, IEEE T. Nucl. Sci., 53(1):304-311.

[4] CARACENA, T.M., *et al.*: A Variable Point Kernel Dosimetry Method for Virtual Reality Simulation Applications in Nuclear Safeguards and Security, IEEE T. Nucl. Sci., 2013, 60(5):3862-3871.

[5] CARACENA, T.M., and VIDAL, E.V., *et al.*: A KD-trees based method for fast radiation source representation for virtual reality dosimetry applications in nuclear safeguards and security, Prog. Nucl. Energy, 2017, 95:78-83.

[6] CHAO, N., LIU, Y.K., and XIA, H., *et al.*: A dose assessment method for arbitrary geometries with virtual reality in the nuclear facilities decommissioning, Radiat. Phys. Chem., 2018, 144:238-247.

[7] CHAO, N., LIU, Y.K., and XIA, H., *et al.*: Adaptive Point Kernel Dose Assessment Method for Cutting Operation of Irregular Geometries in Nuclear Facility Decommissioning, Radiat. Phys. Chem., 2018, 150:125-136.

[8] PARK, H.S., KIM, S.K., and LEE, K.W., *et al.*: The application of visualization and simulation in a dismantling process. J. Nucl. Sci. Technol, 2007, 44:649-656.

[9] KIM, I., CHOI, B., and HYUN, D., *et al.*: A framework for a flexible cutting-process simulation of a nuclear facility decommission, Ann. Nucl. Energy, 2016, 97:204-207.

[10] HYUN, D., KIM, I., and LEE, J., *et al.*: A methodology to simulate the cutting process for a nuclear dismantling simulation based on a digital manufacturing platform, Ann. Nucl. Energy, 2017, 103:369-383.

[11] ZHANG, Y.L., HU, Y.F., and LIU, M., *et al.*: Study of nuclear reactor decommissioning simulation key technologies, nuclear power institute of china, 2015.

[12] PROKHORETS, I.M., and PROKHORETS, S.I., *et al.*: Point-Kernel Method for Radiation Fields Simulation, Probl. Atom. Sci. Tech., 2007, 5:106-109.

[13] SCHŐN, B., MOSA, A.S.M., LAEFER, D.F., and BERTOLOTTO, M.: Octree-based indexing for 3D pointclouds within an Oracle Spatial DBMS. Comput. Geosci., 2013, 51:430-438.